ORIGINAL PAPER

Magnetic and Superconducting Properties of Doped and Undoped Double Perovskite Sr_2YRuO_6

S.M. Rao · J.K. Srivastava · M.K. Wu · B.H. Mok · C.L. Chen · M.C. Ling · H.-L. Liu · Y.Y. Chen · J.C. Ho

Abstract We report here SQUID (magnetization) measurements, along with supporting specific heat, Raman, SEM (scanning electron microscope), EDX (energy dispersive X-ray) and XRD (X-ray diffraction) measurements, on Cu-doped and undoped double perovskite $Sr_2^{2+}Y^{3+}Ru^{5+}O_6^{2-}$ (abbreviated as SrY2116) system grown as single crystal using high-temperature solution growth technique. These measurements show the undoped system to be a nonmetallic (insulating) spin glass (SG) and the $\sim$ 5–30% Cu-doped (i.e. Cu-concentration/(Cu + Ru-concentration) $\sim$ 5–30%) system to be a spin glass superconductor (SGSC) with T_c (critical temperature) $\sim$ 28–31 K and superconducting volume fraction, $f_{sc} \sim$ 2.2–9%. To mention, similar measurements done on undoped and Cu-doped BaY2116 and BaPr2116 systems show for them the same (SG, SGSC) behaviors. However they show a decrease in T_c and f_{sc} when diamagnetic Y^{3+} ions are replaced by Pr^{3+} spins, presumably due to enhanced internal pair breaking, and also decreased Cu–O–Cu overlap, owing to Pr^{3+} presence; these phenomena are known to exist in the Pr123 compound, $PrBa_2Cu_3O_{7-\delta}$ ($\delta \sim$ 0), due to $\sim$ 10% of Pr^{3+} ions having tendency to occupy Ba^{2+} sites. Measurements done on undoped and Cu-doped SrHo2116 show similar SG and SGSC properties. Further, the undoped and Cu-doped SrY2116 crystals grown by hydrothermal growth technique (i.e., grown using lower temperature and high pressure) show same behaviors. From these investigations it can be said that the undoped Ru-double perovskites ($A_2BB'O_6$, B' = Ru) are SG systems and that Cu-doped Ru-double perovskites ($A_2BB'O_\delta$, $\delta \sim$ 6, B' = $Ru_{1-x}Cu_x$, $0 < x \lesssim 0.3$) are SG superconductors (SGSCs). Results are discussed.

Keywords Double perovskite · Ruthenocuprate · High-T_c superconductivity · Magnetic superconductor · Frustration · Spin glass

S.M. Rao · M.K. Wu · B.H. Mok · C.L. Chen · Y.Y. Chen
Institute of Physics, Academia Sinica, Nankang, Taipei 115, Taiwan (ROC)

J.K. Srivastava (✉)
Tata Institute of Fundamental Research, Mumbai 400005, India
e-mail: jks@tifr.res.in

M.K. Wu
Department of Physics and Materials Science Center, National Tsing Hua University, Hsinchu, Taiwan (ROC)

M.C. Ling · H.-L. Liu
Department of Physics, National Taiwan Normal University, Taipei 116, Taiwan (ROC)

J.C. Ho
Department of Physics, Wichita State University, Wichita, KS 67260-0032, USA

1 Introduction

The discovery of superconductivity in Sr_2RuO_4 [1], though at very low temperature, has led to the examination of the magnetism and conductivity of Ru-based oxides [2–14] in an attempt to find out if high-T_c (critical temperature) superconductivity (T_c higher than cuprates) can be obtained in a material without any Cu–O plane. In this paper we report our results obtained on single crystals of undoped and Cu-doped $Sr_2^{2+}Y^{3+}Ru^{5+}O_6^{2-}$ (SrY2116 for brevity), grown from high-temperature solutions, using a variety of techniques like SQUID, specific heat, Raman, SEM (scanning electron microscope), EDX (energy dispersive X-ray), and XRD (X-ray diffraction) measurements. The Cu-doped system can be written as $Sr_2YRu_{1-x}Cu_xO_\delta$ (x = 0–0.3, δ = 6 or $\sim$ 6). Sr_2YRuO_6 (doped or undoped) belongs to the large

family of double perovskites which have been investigated by several groups [15–23]. Battle and Macklin [20] studied polycrystalline samples of SrY2116 prepared by high-temperature sintering of stoichiometric powders. Their high-field (38.1 kOe) magnetization study reports for the system an antiferromagnetic transition temperature (T_N) of ~ 26 K and the neutron diffraction study shows same crystal symmetry, with no drastic change in any lattice parameter, at 4.2 K and room temperature plus an antiferromagnetic ordering of spins at 4.2 K. Wu and coworkers [2–4] investigated polycrystalline samples of $Ba_2YRu_{1-x}Cu_xO_\delta$ and $Sr_2YRu_{1-x}Cu_xO_\delta$ and reported coexistence of superconductivity and magnetism for $x = 0.05$ to 0.2. The magnetic and superconducting properties investigated by us for the $Sr_2YRu_{1-x}Cu_xO_\delta$ single crystals, along with the results of the supporting SEM, EDX, Raman, XRD, and specific heat measurements, bring out the spin glass (SG) and spin glass superconductor (SGSC) nature of the system for different x values. Details are discussed.

2 Experimental

The undoped and Cu-doped SrY2116 powders were prepared by the solid-state reaction of a stoichiometric mixture of $SrCO_3$ (or SrO), Y_2O_3, RuO_2, and CuO constituent materials. These constituents (in powder form) were made to react in air at $1050\,°C$ for three times to ensure completion of the reaction which was confirmed by powder X-ray diffraction analysis. Crystals were grown from high-temperature solutions. The solvent consisted of a 50:50 mixture of $PbO:PbF_2$ (flux). The solute, SrY2116 powder (undoped or Cu doped), with a weight of ~ 10–20% of $PbO:PbF_2$ mixture weight, was added to the solvent. The solute and solvent, ~ 3–6 grams, were thoroughly mixed and packed in a platinum crucible covered with a platinum lid. The crucible was placed in the crystal growing furnace which could be heated by programmed heating to melt the solvent–solute mixture, soak and grow crystals by slow cooling. The slow cooling was done from several temperatures (called growth temperature (GT)) in the range 1125 to $1200\,°C$. As is explained later, the results presented in this paper are for the crystals grown at $1135\,°C$ (i.e., GT $= 1135\,°C$), where good results were obtained. In this case (i.e., in $1135\,°C$ GT crystals's case), the solute-solvent mixture was heated to $1135\,°C$, soaked for 6–8 hours to homogenize, and then cooled at the rate of 0.2 to $0.5\,°C$ per hour to $1120\,°C$. From there the crucible was cooled at a faster rate (50–$150\,°C$ per hour) to room temperature. Finally, the crucible was removed from the furnace, excess flux was drained off, and crystals were taken out. During the crystal growth (i.e., during 1135–$1120\,°C$ cooling period), the crucible was rotated clockwise and anticlockwise at 20–25

rpm with a hold time, between reversals, of 30–40 seconds. Typical growth program took nearly 3–5 days. The magnetic and superconducting properties of the grown crystals (called "as grown" crystals) were investigated using SQUID magnetometer. Due to the small size of the crystals (octahedra measuring 1–3 mm along body diagonal), we could not carry out the resistivity measurements. We have also done measurements on these "as grown" crystals after annealing them in gas atmospheres. However, those measurements did not give any significantly new result and therefore are not described here.

Measurements have been done using commercial equipments. The SQUID magnetometer used in the measurement was of Quantum Design make. The SEM and EDX measurements were made using a JOEL Model-840 SEM operating at 20 kV in conjunction with an Oxford Model LINK eXL EDX analyzer. The XRD measurements were performed with Phillips X-ray Diffractometer Model PW-3040/60 using monochromatic CuK_α radiation. The specific heat measurements were carried out using a Quantum Design PPMS (Physical Property Measurement System). The Raman measurements were performed on a Dilor XY 800 spectrometer using the 5145 Å excitation line from an Ar^+-ion laser.

Since commercial SQUID magnetometers often have a trapped magnetic field, which is opposed to the applied field, in some cases they can show erroneous result like showing negative magnetization ($-M$) in a zero-field-cooled measurement as the zero-field-cooled state there actually becomes a small negative-field-cooled state. In order to make sure that such a problem does not exist in our case, we have taken good care to see that the so-called trapped flux or remanent field is not influencing our measurements. For this, we took precautions as per the manufacturer's recommendations, following which the system is degaussed first without the sample and then with the sample present in the system. For the first degaussing, the system is taken to 300 K and degaussed using the standard instrument sequence after which the remanent field is generally zero. In addition, another degaussing is done with alternating negative and positive fields in the range 50 to 0 Oe in different steps. This helps in removing the effects due to the fields used by the previous user. Sample is now inserted in the cavity, heated to 350 K, and degaussed with alternating negative and positive fields in the range 50 to 0 Oe. This provides additional protection against any stray field effect on sample magnetization.

3 Results and Discussion

Figure 1 shows some typical results of SEM, EDX, Raman, and XRD measurements. Figure 1(a) shows a typical as grown crystal. The morphology of the crystals depended on the composition of $PbO:PbF_2$ mixture. For a 50:50 composition octahedral crystals were obtained (Fig. 1(a)), and
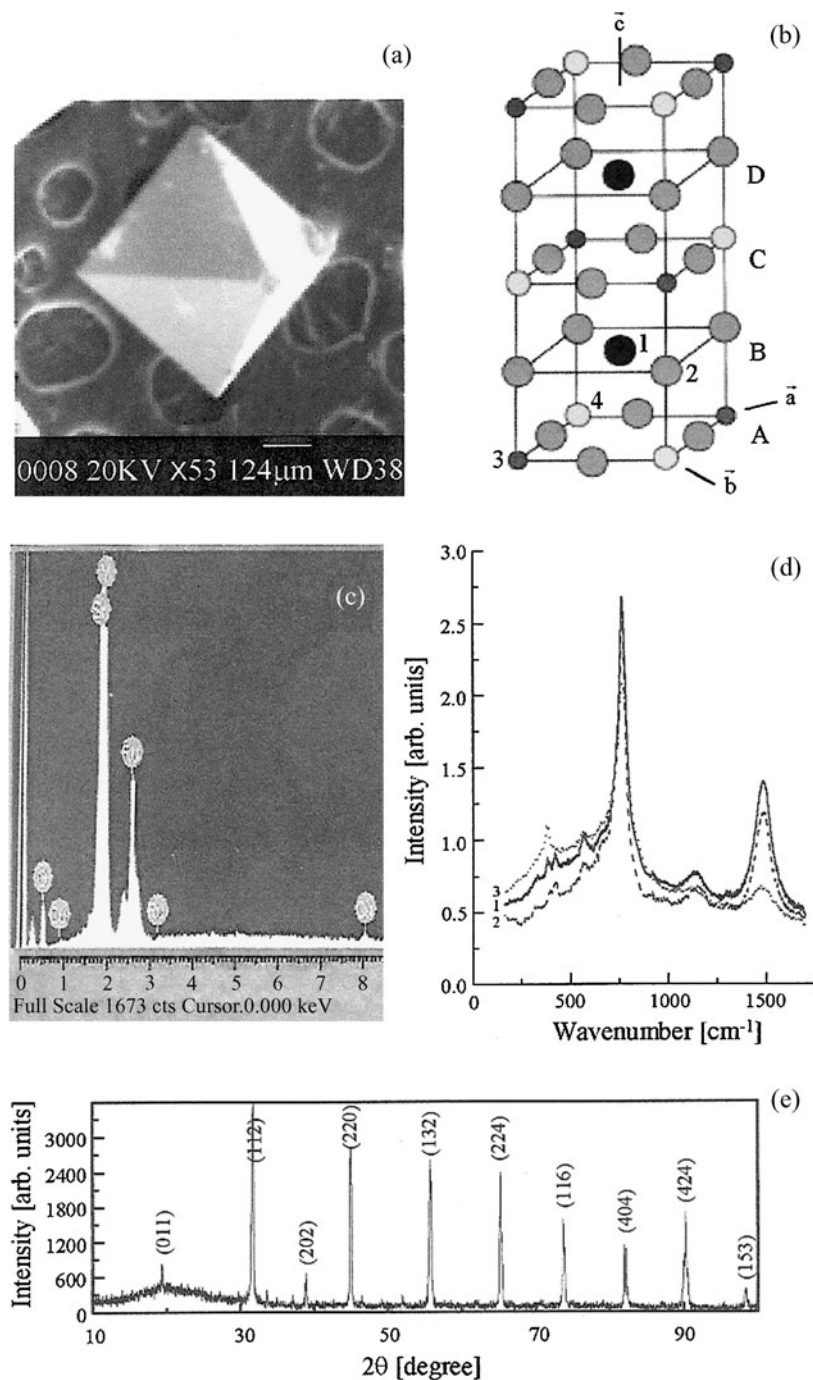
Fig. 1 (**a**) A typical crystal habit (SEM micrograph). The crystal shown is an as grown $Sr_2YRu_{1-x}Cu_xO_\delta$ crystal ($x = 0.1$, GT (growth temperature) = 1135 °C). (**b**) Crystal structure of Sr_2YRuO_6; the ion positions are 1 = Sr, 2 = O, 3 = Ru (predominantly), 4 = Y (predominantly). A, B, C, D, are the various planes, and $\vec{a}$, $\vec{b}$, $\vec{c}$ the crystallographic axes. (**c**) EDX spectrum (intensity [arbitrary units] vs. energy [keV]) of as grown, GT = 1135 °C, $Sr_2YRu_{1-x}Cu_xO_\delta$ ($x = 0.1$) system. The writings in the figure, from left to right, are O, Cu, Sr, Y, Ru, Ru, Cu. (**d**) Raman spectrum (intensity vs. Raman shift) recorded for the as grown, GT = 1135 °C, $Sr_2YRu_{1-x}Cu_xO_\delta$ system ($x = 0$ (*curve 1*), 0.1 (*curve 2*), and 0.3 (*curve 3*)). (**e**) Powder X-ray diffraction pattern recorded for powdered as grown, GT = 1135 °C, $Sr_2YRu_{1-x}Cu_xO_\delta$ ($x = 0.1$) single crystal

for a 40:60 composition, the crystals were flatter plate like (in which the corners of the octahedra were absent). However, the properties (structural, magnetic, and superconducting) of the crystal did not depend on its morphology. The

superconducting critical temperature T_c and superconducting volume fraction f_{sc}, obtained from the SQUID data using the procedure described in [3], were found to depend on x (Fig. 2) and GT. The results described in this pa-
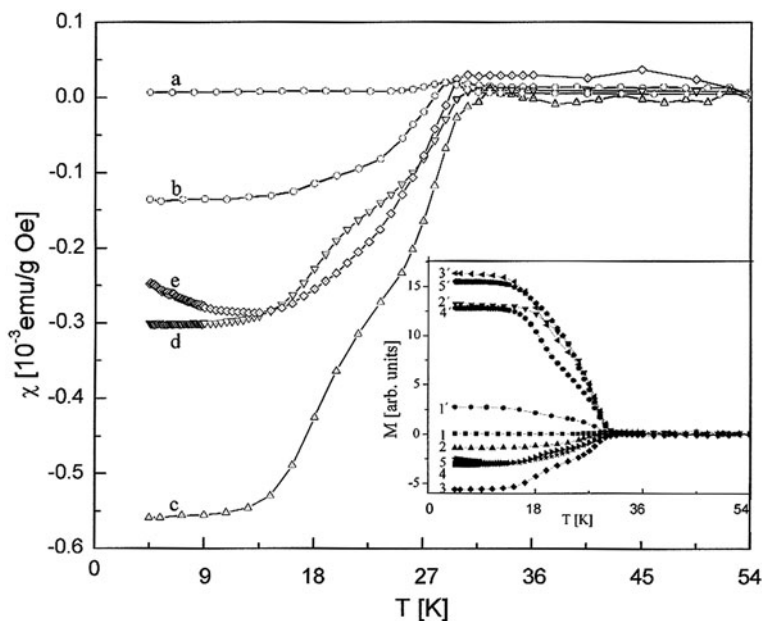
Fig. 2 Susceptibility (χ) as a function of temperature (T) for as grown (GT = 1135 °C) $Sr_2YRu_{1-x}Cu_xO_\delta$ ($x = 0$ (*curve a*), 0.05 (*curve b*), 0.1 (*curve c*), 0.2 (*curve d*), 0.3 (*curve e*)) system; $\chi = M$ (magnetization)/H (external magnetic field), $H = 10$ Oe. *Curves a, b, c, d, e* are zero-field-cooled (ZFC) curves. In the *inset*, FC (field cooled) curves (*curves 1′, 2′, 3′, 4′, 5′*) are also shown along with the ZFC curves (*curves 1, 2, 3, 4, 5*); $x = 0$ (*curves 1, 1′*), 0.05 (*curves 2, 2′*), 0.1 (*curves 3, 3′*), 0.2 (*curves 4, 4′*) and 0.3 (*curves 5, 5′*). For

recording the ZFC–FC curve, sample has been first cooled in zero field to lowest T and H (10 Oe) applied there. With H present, M vs. T has been recorded up to 300 K (room temperature) (ZFC curve). After that the sample has been cooled back in the same H to lowest T and M vs. T recorded again with T increasing and H present (FC curve). It may be mentioned that same FC curve is obtained whether it is recoded with T increasing or decreasing

per (Figs. 1–8), unless specifically mentioned otherwise, are for as grown crystals having GT = 1135 °C and compositions $x = 0.1$, where T_c and f_{sc} are maximum (Fig. 2), and $x = 0$ (which is the undoped crystal studied for comparison). Figure 1(b) shows the SrY2116 crystal structure, Fig. 1(c) shows the results of EDX measurement for $x = 0.1$, and Fig. 1(d) shows Raman spectra recorded for $x = 0$, 0.1, and 0.3. The Cu peaks in Fig. 1(c) show the incorporation of Cu in the doped lattice. Raman investigations also confirm the incorporation of Cu in the doped crystal by showing a change in the spectrum with x (Fig. 1(d)). All the samples were investigated by X-ray diffraction, and Fig. 1(e) gives a typical XRD pattern obtained for $x = 0.1$ sample. The peak positions shift, though by small amount, to higher (lower) θ values with increasing (decreasing) x. Analysis of these patterns yields lattice parameters for $x = 0$ as $a = 5.775(8)$ Å, $b = 5.772(4)$ Å, $c = 8.138(7)$ Å, and $\beta = 90.0(1)°$, showing monoclinic structure (space group $P2_1/n$) in agreement with the published data [20], and for $x = 0.1$ as $a = 5.712(6)$ Å, $b = 5.711(3)$ Å, $c = 8.116(3)$ Å, and $\beta = 89.9(9)°$. Table 1 gives, for different x, typical XRD and Raman peak positions, T_c and f_{sc}. As seen there, Raman peak positions shift to higher frequencies, indicating a decrease in bond length, with increasing x. This is consistent with the decrease shown by the XRD measurements in

lattice parameters as x increases. Table 2 presents the EDX analysis results.

Figure 3(A) shows the M (magnetization)–T (temperature) curve recorded for $x = 0$ sample; curve a is for ZFC (zero-field-cooled) sample, and curve b is for FC (field-cooled) sample and H (external magnetic field) = 50 Oe. The natures of ZFC (curve a) and FC (curve b) curves, like the presence of magnetic irreversibility M_{irr} (branching of ZFC and FC magnetization (M(ZFC), M(FC)) curves) below $\sim$ 32 K, indicate that the $x = 0$ sample is probably a reentrant SG [24–29]. As we will see later, further data (Figs. 3–7) and their analysis seem to confirm it. For instance, in Fig. 3(A) and more clearly in its insets (i) and (ii), we find that in curves a, b the magnetization starts increasing suddenly at $\sim$ 35 K (T_1), then at $\sim$ 32 K (T_2) curve a has a peak, and curves a, b have start of M_{irr}, and finally at $\sim$ 20 K (T_3) there is a hump in curve a and step in curve b. We call T_1 as T_C (ferrimagnetic Curie temperature) since we find the presence of magnetic hysteresis curve below T_1 (Fig. 6) and its absence above T_1. The T_1 cannot be identified with a ferromagnetic transition temperature since neutron diffraction measurements have shown antiparallel alignment of spins below T_1 [20]. This antiparallel alignment of spins, as we will discuss later, is ferrimagnetic, and not antiferromagnetic, in nature. We also find that above T_1, a mild M_{irr} exists (Fig. 3(A), inset (ii)) and M–H variation is nonlin-

Table 1 Values of largest amplitude Raman peak's position (RPP), largest amplitude XRD peak's position (XRDPP), critical temperature (T_c (onset)) and superconducting volume fraction (f_{sc}) for different x in $Sr_2YRu_{1-x}Cu_xO_\delta$ system

| x	RPP [cm^{-1}]	XRDPP (2θ [degree])	T_c [K]	f_{sc} [%]
0	761.3	30.98	–	–
0.05	762.1	31.01	27.8	2.2
0.1	762.9	31.30	31.0	9.0
0.2	764.1	31.40	29.8	4.9
0.3	765.2	31.51	28.9	4.6

Table 2 Results of EDX analysis for elements' percentage in $Sr_2YRu_{1-x}Cu_xO_\delta$ system

$x = 0$			$x = 0.1$		
Element	Weight %	Atomic %	Element	Weight %	Atomic %
O	21.38	60.87	O	20.12	58.76
Cu	–	–	Cu	1.24	0.91
Sr	37.16	19.32	Sr	39.90	21.28
Y	19.25	9.86	Y	18.89	9.93
Ru	22.21	9.95	Ru	19.85	9.12
Total	100.00	100.00	Total	100.00	100.00

ear (Fig. 4(A)). The nonlinearity persists up to 300 K, our highest measurement temperature, and can be seen clearly by M/H vs. H plot since for a linear $M–H$ variation, M/H will not change with H. This nonlinearity and the mild M_{irr} above T_C (T_1) indicate the presence of magnetic clusters in the otherwise paramagnetic system. The fact that no magnetic hysteresis is seen by us above T_C is consistent with the neutron diffraction measurement of Battle and Macklin [20], which shows the absence of any long-range magnetic ordering in SrY2116 at room temperature. Such a behavior (presence of clusters and no long-range ordering above a certain temperature) has been seen in SG systems [24, 25, 30, 31]. As we will show later, T_2 and T_3 can be associated with SG transition in $x = 0$ system. Because of their SG transition nature, T_2 and T_3 transitions shift to lower temperatures with increasing H (Fig. 7) [24–29]. Thus, the ~ 26 K transition observed in high field, which was thought to be T_N (Néel temperature) by Battle and Macklin [20], is actually the T_2 transition which has shifted to lower temperature in large H (Fig. 4(A), inset (ii)). In a reentrant SG system there are four transition temperatures, namely T_{CF}, T_C or T_N, T_{M1}, and T_{M2}; normally $T_{CF} > T_C$, $T_N > T_{M1} > T_{M2}$ (but near tricritical point, the T_C and T_{M1} may be quite close) [24–29]. As one cools the lattice, at T_{CF} magnetic clusters are formed in the material's otherwise paramagnetic state. The magnetic ordering inside clusters can be ferro-, ferri-, or antiferromagnetic. Assigning a spin $\vec{S}_{cl}$ to a cluster (lattice/sublattice), at T_C or T_N the z-component of $\vec{S}_{cl}$, $(\vec{S}_{cl})_z$, of all clusters get magnetically ordered, and the x-, y-components $(\vec{S}_{cl})_x$, $(\vec{S}_{cl})_y$ average out to zero; T_N = Néel temperature, T_C = ferro- or ferrimagnetic Curie temperature. On further cool-

ing, at T_{M1} $(\vec{S}_{cl})_z$ remain magnetically ordered, but $(\vec{S}_{cl})_x$, $(\vec{S}_{cl})_y$ freeze in SG configuration (random direction pointing on the average). Finally at T_{M2}, all the three components, $(\vec{S}_{cl})_z$, $(\vec{S}_{cl})_x$, $(\vec{S}_{cl})_y$, get randomly frozen in SG configuration. From the discussions above we conclude that for $x = 0$ sample, $T_{CF} > 300$ K, $T_C \sim 35$ K (T_1), $T_{M1} \sim 32$ K (T_2), and $T_{M2} \sim 20$ K (T_3). The above conclusion also is supported by the specific heat measurements (Fig. 5, curve a). We find no specific heat (C) anomaly at T_2, T_3 transition temperatures (Fig. 5). This supports the SG nature of T_2 (T_{M1}), T_3 (T_{M2}) transitions since specific heat is known not to show any anomaly at SG (random freezing) transitions [26–29, 32, 33]. Further, due to the closeness of T_C (T_1) and T_{M1} (T_2), we also do not see any C anomaly at T_C. SG (T_{M1}, T_{M2}) transitions have width and can mask any effect of T_C transition on C due to T_C, T_{M1} closeness. In Fig. 5, curve a ($x = 0$), we see that when plotted as C/T vs. T^2, the data show a sharp increase in the C/T value at very low temperatures ($\lesssim 1$ K). Such an increase shows the presence of magnetic clusters in the system [34, 35]. We find that this SG nature, with magnetic clusters, is present in all the samples studied by us for $0 \leq x \leq 0.3$. In addition, the samples with $x = 0.05$–0.3 also show the presence of superconductivity (Fig. 2). As an example, we discuss below the results of the $x = 0.1$ sample.

Figure 3(B) shows the $M–T$ curve for $x = 0.1$ sample (ZFC curve (curve a), FC curve (curve b), $H = 10$ Oe). A careful examination of the curves a, b shows that using the criteria discussed above (for $x = 0$ case), for $x = 0.1$ case, we can write $T_C \sim 35$ K (from where M starts suddenly increasing), $T_{M1} \sim 32$ K (where M_{irr} is seen), and
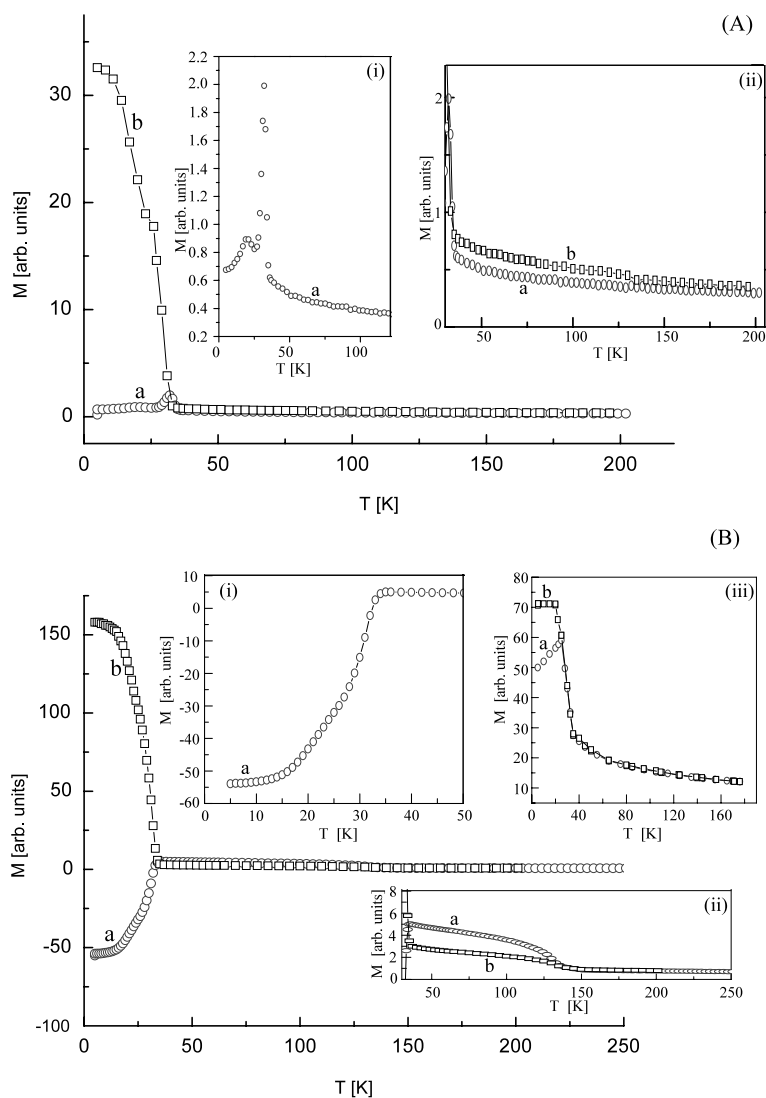
Fig. 3 Temperature (T) dependence of magnetization (M) for as grown, GT = 1135 °C, $Sr_2YRu_{1-x}Cu_xO_\delta$; *curve a* is for ZFC case, and *b* for FC case. (**A**) $x = 0$, H (external field) = 50 Oe. *Inset (i)* shows enlarged view of a portion of *curve a* and *inset (ii)* shows the same for the *curves a, b* high T portions. (**B**) $x = 0.1$, $H = 10$ Oe for main figure plus *insets (i), (ii)* and 2 kOe for *inset (iii)*. *Inset (i)* shows enlarged view of a *curve a* portion, and *inset (ii)* shows the same for *curves a, b* high T portions. The *inset (iii)* shows ZFC-FC curves recorded for $H = 2$ kOe

$T_{M2} \sim 19$ K (where curves a, b show humps). At T_{M1} the ZFC curve (curve a) has a small peak which can be seen more clearly in Fig. 7(A). Similarly, the T_{M2} hump and the T_C increase of M can be seen more clearly in Figs. 2, 7. As for the $x = 0$ case, here also mild M_{irr} (Fig. 3(B), inset (ii)) and nonlinear $M–H$ variation (Fig. 4(B)) are present above T_C. The nonlinearity exists up to our highest measurement temperature (~ 300 K). This indicates that also for $x = 0.1$ case, $T_{CF} > 300$ K. Magnetic hysteresis is present below T_C (Fig. 6) and absent above T_C, showing ferrimagnetic Curie temperature nature of T_C. Like for the case of $x = 0$ sample, the specific heat measurement confirms the presence of clusters up to the lowest measurement temperature (Fig. 5, curve b). The long-range magnetic ordering and

SG freezing via frustrated intercluster interaction have been concluded to be also present in some other systems [36]. Similar to the $x = 0$ case, here the specific heat measurement (Fig. 5, curve b) also shows no C anomaly at T_C, T_{M1}, or T_{M2}. Figure 3(B), inset (iii), shows the $M–T$ behavior for $x = 0.1$ sample in large H ($H = 2$ kOe). For this case, the transition temperatures have shifted and are $T_{M2} < 5$ K (our lowest measurement T), $T_{M1} \sim 25$ K (beginning of M_{irr}), and $T_C \sim 35$ K (from where M has sudden rise as can be seen by extrapolation of the rising curve's almost vertical linear portion; the start of enhanced M increase from ~ 60 K is due to the enhanced polarization of the paramagnetic spins (clusters) above T_C by large H). Such H effect is known to occur in SG systems confirming the SG nature of
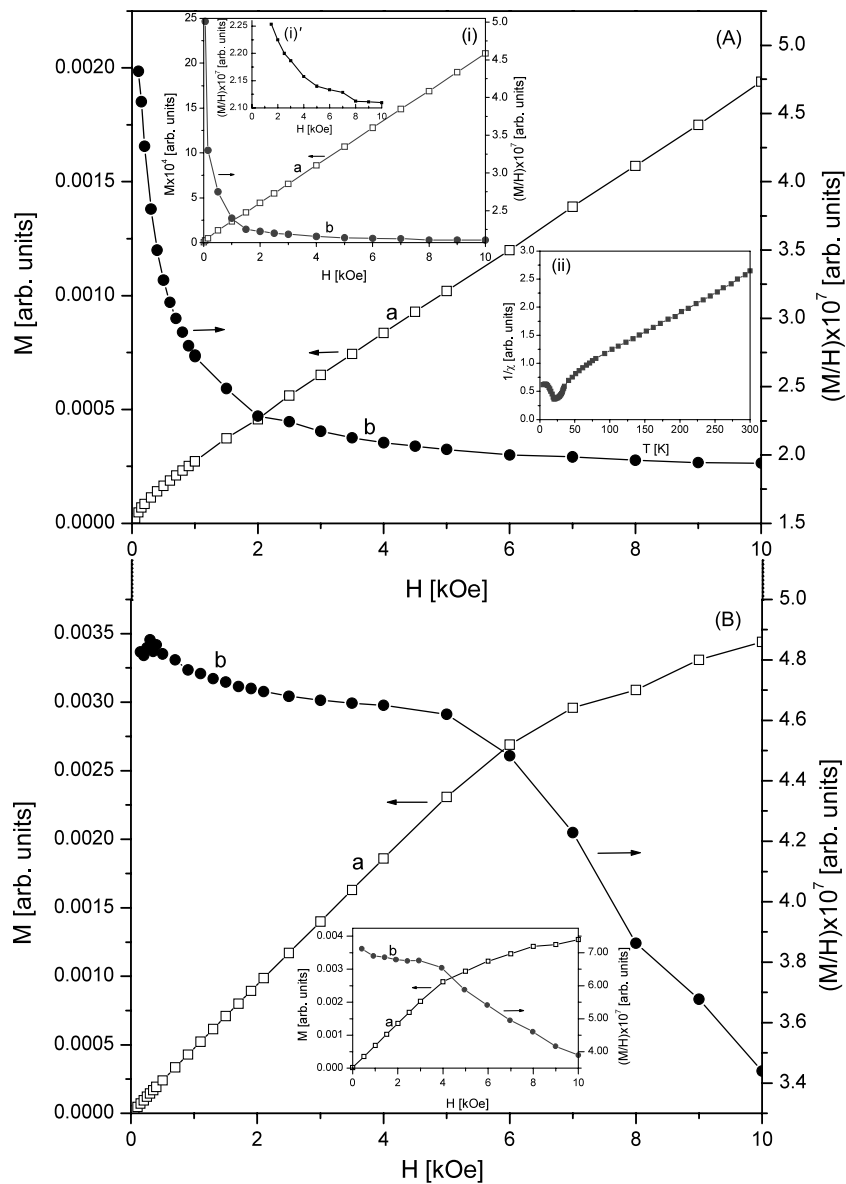
Fig. 4 *M* (magnetization), *M/H* vs. *H* (external magnetic field) for as grown, GT = 1135 °C, $Sr_2YRu_{1-x}Cu_xO_\delta$ system (zero-field-cooled); $x = 0$ (**A**), 0.1 (**B**). Temperature $T = 250$ K for the main figures ((**A**), (**B**), main portions) and $T = 100$ K for (**A**), *inset (i)*, and (**B**), *inset*.

As shown by the *arrows*, *left-hand* (*right-hand*) *side y-axis* scale is for *open* (*filled*) data points. An enlarged view of a (**A**), *inset (i)*, *curve b* portion is shown in *inset (i)′*. (**A**), *inset (ii)*, shows $1/\chi$ vs. *T* curve recorded for $H = 5$ kOe; χ (susceptibility) $= M/H$

the T_{M1}, T_{M2} transitions [24–29, 37–41]. As seen from the Fig. 3(B) curve a, the $x = 0.1$ system has one more transition temperature which is absent for $x = 0$ system (Fig. 3(A), curve a). This is the superconducting transition temperature $T_c \sim 31$ K (from where M in curve a becomes negative indicating start of diamagnetic transition (T_c onset)). Like T_{M1} and T_{M2}, T_c also decreases to lower value with increasing H (Fig. 7). This is consistent with the known T_c vs. H behavior [4, 42, 43]. Like the case of T_C, the closeness of T_c and T_{M1} is responsible for the specific heat measurement not showing any anomaly at T_c (Fig. 5, curve b). Thus the $x = 0.1$

system can be called a spin-glass superconductor (SGSC). It may be mentioned here that though the M–T data given in Fig. 3(A) ($x = 0$) are for $H = 50$ Oe, same M–T results are also obtained for $H = 10$ Oe. However the SG transition temperatures are more clearly visible for $H = 50$ Oe case as the M signal is large there due to larger H. We have not given the $x = 0$ $H = 10$ Oe M–T curves (ZFC, FC) here since in Fig. 2 we have already shown the χ vs. T behavior for various x, including $x = 0$, 0.1, for $H = 10$ Oe. As shown there, $-M$ is observed only for $x \neq 0$ samples, including $x = 0.1$ sample, but not for $x = 0$ sample, which shows $+M$ at all T. This is also true for other H.

Fig. 5 Temperature (T) dependence of the specific heat (C) plotted as C/T vs. T for the as grown, GT = 1135 °C, $Sr_2YRu_{1-x}Cu_xO_\delta$ (zero-field-cooled); $x = 0$ (*curve a*), $x = 0.1$ (*curve b*), H (external field) = 0. *Inset (i)* (C/T vs. T) and *inset (ii)* (C/T vs. T^2) show expanded views of *curves a, b* low-temperature ($T < 3.5$ K) portions
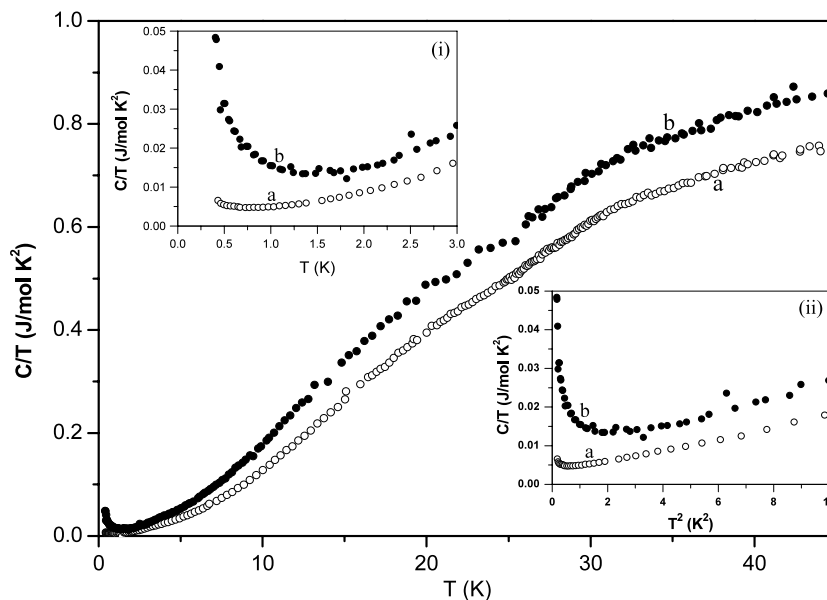

The SG nature of $x = 0, 0.1$ samples is also confirmed by the magnetic hysteresis measurement (Fig. 6). In Fig. 6(A), inset (ii), coercive field H_c, obtained from hysteresis loops, vs. T is plotted for $x = 0, 0.1$ cases, and in both cases, maximum H_c occurs at an intermediate temperature (below and above which H_c is lower). This is a known behavior in SG systems [30, 31]. In Fig. 6(B) ($x = 0.1$), a large $-H$ shift is seen in the hysteresis curve center on field cooling (curve a (ZFC), curve b (FC)). This is known to be an SG system's property [26–31]. Further, the inset in Fig. 6(B) shows a typical time (t) variation of ZFC magnetization (M(ZFC)) for $x = 0.1$ sample. Such a time variation is known to occur in SG systems [24–29]. In Fig. 6(B) the fact that just a 100 Oe field cooling gives a large $-H$ shift, of ∼ 3.64 kOe, to the ZFC hysteresis loop center indicates the involvement of clusters, as clusters will get affected even by a small field.

The origin of the SG behavior of $x = 0$ sample and SGSC nature of $x = 0.1$ sample can be understood as follows. For the $x = 0$ case (Fig. 1(b)), if all the Ru ions (Ru^{5+} (4d^3, $S = 3/2$)) occupied unit cell site 3, and all the Y ions (Y^{3+} (diamagnetic)) occupied unit cell site 4 in the lattice, an uniform distribution of cations would have existed resulting in an uniform antiferromagnetic ordering as was thought to be the case by Battle and Macklin [20]. However, even if small amount of Ru and Y ions have got randomly substituted at each other's site, which is possible [26–31], magnetic frustration would occur in the lattice, owing to a difference in Ru^{5+} (1.85 μB), Y^{3+} (0 μB) moments [20], making the system a reentrant SG [26–29, 37–41]. Even a small Ru, Y mixing is enough to cause the effect since once the frustration develops at a site, it propagates in the lattice by affecting the neighboring spins. At T_C the ordering will be ferrimagnetic owing to the presence of antiparallely aligned spins on

neighboring, say A, C, planes (Fig. 1(b)) [17–20] that will have net unequal moments due to the presence of Y^{3+} in different numbers in these planes because of the Ru, Y random mixing.

The $x = 0$ system ($Sr_2^{2+}Y^{3+}Ru^{5+}O_6^{2-}$) is an insulator. When Cu is introduced in this system, as in $x = 0.1$ sample, it presumably goes to the Ru site (ionic size effect), and the system becomes $Sr_2YRu_{1-x}Cu_xO_\delta$ [4]. As in cuprates, Cu goes in the lattice in both Cu^{2+} and Cu^{3+} charge states and to maintain the charge neutrality, Ru^{4+} is created along with Ru^{5+} [8–10]. The $x \neq 0$ system becomes metallic presumably due to the Cu$^{2+} \rightleftarrows$ Cu^{3+} charge fluctuation presence as in cuprates [9, 10, 44, 45]. Whether Ru$^{4+} \rightleftarrows$ Ru^{5+} charge fluctuation also exists cannot be said in the absence of detailed band structure calculations. However, presence of several ions with different magnetic moments (Cu^{2+}, Cu^{3+}, Ru^{4+}, Ru^{5+}, Y^{3+}), whether in high or low spin states [8–10] or diamagnetic state, gives rise to additional frustration in the lattice. This makes the average cluster sizes and cluster size distributions for the $x = 0$ and 0.1 systems different. As with the magnetic ordering [17–19, 23], a plane–plane interaction (like A–C coupling via B (Fig. 1(b))) can make the clusters three-dimensional in nature.

From the details given so far we see that $x = 0$ sample is an SG and $x = 0.1$ sample is an SGSC. These SG and SGSC natures of the $x = 0$ and 0.1 samples are also brought out by the H dependence of their $M-T$ curves (Fig. 7). We have associated before, in Fig. 3(B) discussion, the peak seen at ∼ 32 K in ZFC curves of $x = 0.1$ sample (Fig. 7(A)) with T_{M1} transition. With increasing H, an SG (T_{M1} or T_{M2}) peak is supposed to broaden, decrease in height, and shift to lower temperature [24–29, 37–41]. However, the $T_{M1} \sim 32$ K peak of $x = 0.1$ sample's ZFC curve (Fig. 7(A); Fig. 7(A), inset), with increasing H, though broadens and shifts to lower
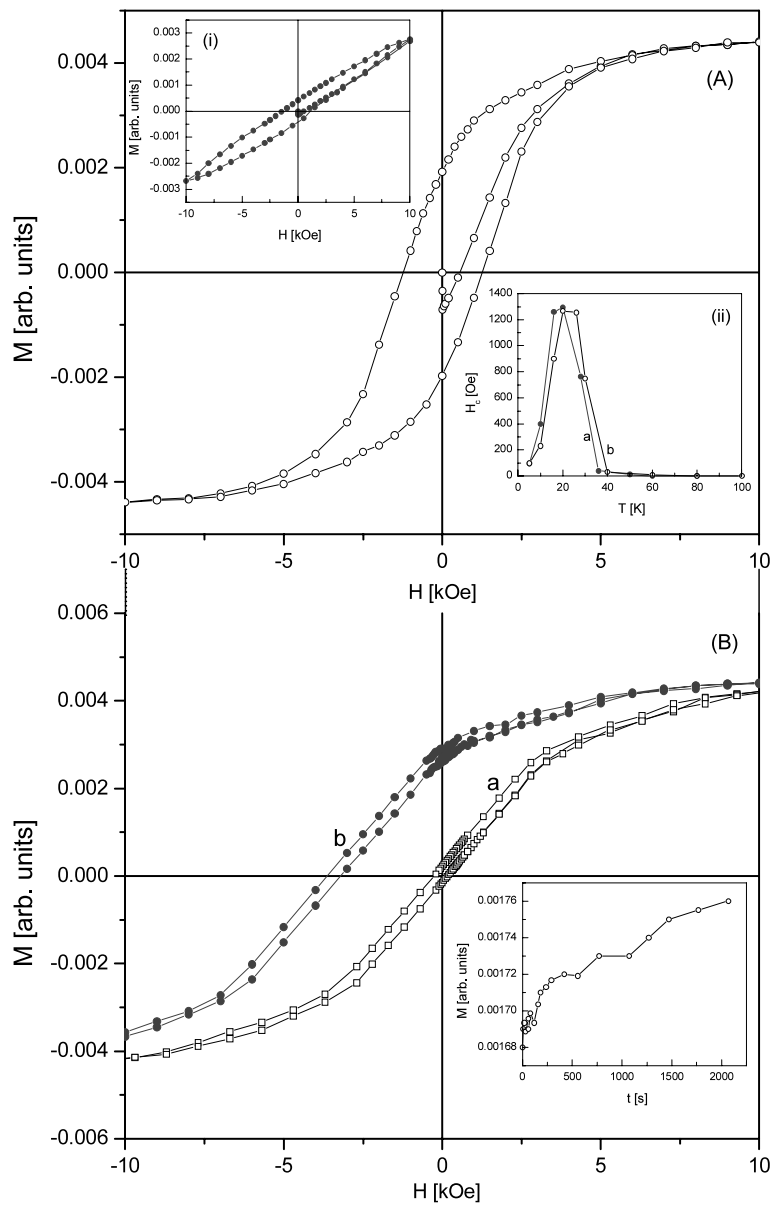
Fig. 6 Magnetic hysteresis curve recorded for the as grown, GT = 1135 °C, $Sr_2YRu_{1-x}Cu_xO_\delta$ system; $x = 0$ ((**A**), *inset (i)*; (**A**), *inset (ii)*, *curve a*), 0.1 ((**A**); (**A**), *inset (ii)*, *curve b*; (**B**); (**B**), *inset*) (M = magnetization, H = external magnetic field, T = temperature, t = time). In (**A**), hysteresis curves are given for zero-field-cooled (ZFC) samples; $T = 26$ K in main figure and 16 K in *inset (i)*. (**A**), *inset (ii)*, shows coercive field, H_c, vs. T for $x = 0$ (*curve a*), 0.1 (*curve b*). In (**B**), $T = 10$ K, *curve a* is ZFC, and *curve b* is FC (field cooled) magnetic hysteresis curve. The *curve b* has been recorded after cooling the sample in $H = 100$ Oe from 300 K (room temperature). (**B**), inset, shows M vs. t curve for ZFC sample recorded at $T = 5$ K in $H = 500$ Oe

temperature, shows oscillation in amplitude (i.e., in peak height above its background). This is seen more clearly in Fig. 7(C) and Fig. 7(C), inset (i), where $M(T)/M$ (80 K) vs. T is plotted so that the background increase with H gets normalized. Thus, the $T_{M1} \sim 32$ K peak of $x = 0.1$ sample is not a pure SG peak. We will show below that this peak is actually an SGSC peak. In Fig. 7(C), inset (ii), we have shown the H dependence of the $x = 0$ sample's $T_{M1} \sim 32$ K peak (Fig. 3(A), curve a) by plotting $M(T)/M$

(80 K) vs. T. As we see there, this peak broadens, decreases in height and shifts to lower temperature with increasing H. Thus it is a pure SG peak. This demonstrates the SG nature of the $x = 0$ sample. We now show the SGSC origin of the $x = 0.1$ $T_{M1} \sim 32$ K peak. The inset in Fig. 7(B) shows a typical reentrant SG system's ZFC (curve a) and FC (curve b) $M-T$ curves, where T_C, T_{M1}, and T_{M2} transitions are shown by arrows ($T_C > T_{M1} > T_{M2}$) [24–29, 37–41]. It also shows typical ZFC (curve c) and FC (curve d)
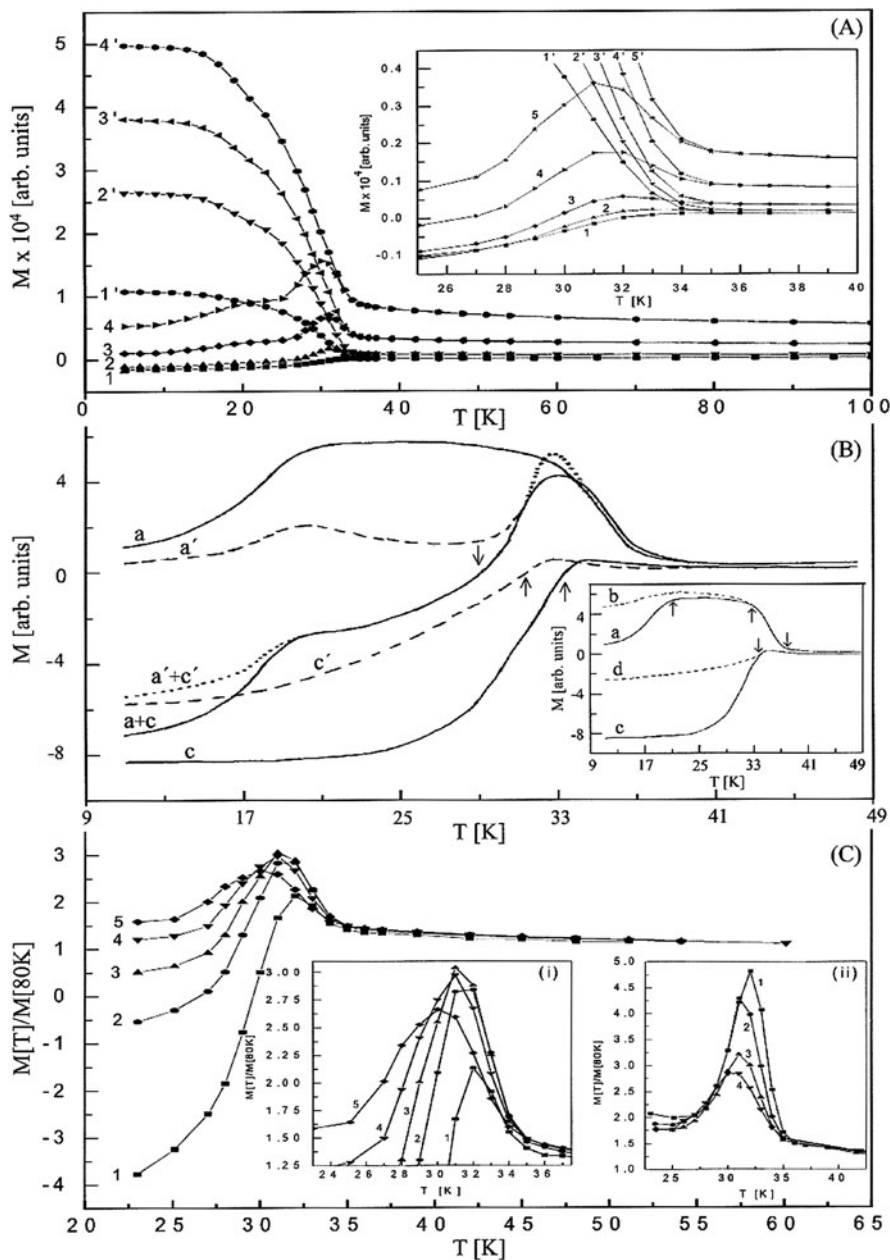
Fig. 7 Temperature (T) dependence of M (magnetization) and $M(T)/M$ (80 K) for as grown, GT = 1135 °C, $Sr_2YRu_{1-x}Cu_xO_\delta$ system; $x = 0$ ((**C**), *inset (ii)*), 0.1 ((**A**); (**A**), *inset*; (**C**); (**C**), *inset (i)*). In (**A**), *curves 1, 2, 3, 4* are for zero-field-cooled (ZFC) case, and *curves 1', 2', 3', 4'* are for field-cooled (FC) case; H (external magnetic field) = 5 Oe (*curves 1, 1'*), 50 Oe (*curves 2, 2'*), 200 Oe (*curves 3, 3'*), and 500 Oe (*curves 4, 4'*). In (**A**), *inset, curves 1, 2, 3, 4, 5* are for ZFC case, and *curves 1', 2', 3', 4', 5'* are for FC case; $H = 5$ Oe (*curves 1, 1'*), 10 Oe (*curves 2, 2'*), 20 Oe (*curves 3, 3'*), 50 Oe (*curves 4, 4'*), and 100 Oe (*curves 5, 5'*). (**A**), *inset*, shows enlarged view, near peak region, of the M–T variation shown in (**A**), main portion, at several H. In (**C**) and (**C**), *inset (i)*, *curves 1, 2, 3, 4, 5* are for ZFC case; $H = 20$ Oe (*curve 1*), 50 Oe (*curve 2*), 100 Oe (*curve 3*), 200 Oe (*curve 4*), and 500 Oe (*curve 5*). In (**C**), *inset (ii)*, *curves 1, 2, 3, 4* are for ZFC case; $H = 50$ Oe (*curve 1*), 200 Oe (*curve 2*), 500 Oe (*curve 3*), and 1000 Oe (*curve 4*). (**C**) shows $M(T)/M$ (80 K) vs. T behavior; $M(T)/M$ (80 K)

$\equiv \chi(T)/\chi$ (80 K), χ (susceptibility) $= M/H$. (**C**), *inset (i)*, shows enlarged view of a portion of (**C**), main figure. (**B**) is a theoretical plot. In (**B**), *inset*, typical M–T curves are given for a reentrant spin-glass (SG) system (*curve a* (ZFC case), *curve b* (FC case)) and a superconductor (SC) (*curve c* (ZFC case), *curve d* (FC case)). The arrows in *curves a, b* represent, starting from high T side, T_C (Curie temperature), T_{M1} (first SG transition temperature (SGTT)), and T_{M2} (second SGTT). The arrow in the *curves c, d* represents T_c (critical temperature). In (**B**), main portion, *curves a, c* are shown along with their sum curve (*curve a + c*); *curve a + c = curve a + curve c* (i.e., at any T, M of curve a + c, $M_{a+c} = M_a$ (*curve a M* value) + M_c (*curve c M* value)). In addition, *curves a' and c'*, showing another type of ZFC SG and SC M–T curves, are also given there along with their sum curve (*curve a' + c'*). The three arrows in the main figure, starting from high T side, represent T_c of *curves c, c' and a + c, a' + c'*. Details are discussed in the text
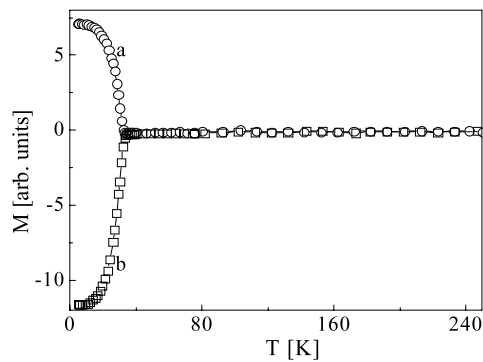
Fig. 8 Temperature (T) dependence of magnetization (M) for as grown, GT = 1135 °C, $Sr_2YRu_{1-x}Cu_xO_\delta$, $x = 0.1$. *Curve a* is for ZFC case, *curve b* for FC case and H (external magnetic field) = −10 Oe

M–T curves of an SC (superconductor) system with T_c (onset) marked by arrow [46–48]. In an SGSC system, the observed ZFC M–T curve is a sum (superposition) of curve a and curve c. In the main portion of Fig. 7(B), curves a and c are shown more clearly, and their sum curve (curve a + c) is also shown. This (curve a + c) is the ZFC M–T curve of an SGSC system. It has a peak near T_c, which represents the $x = 0.1$ $T_{M1} \sim 32$ K SGSC peak, and a hump at low temperature which represents the $x = 0.1$ $T_{M2} \sim 19$ K SGSC peak. For some reentrant SG systems, depending on the H value used and the sample nature, the ZFC M–T curve looks like curve a′ (Fig. 7(B)) with peaks present at T_{M1}, T_{M2} as, for instance, is the case in Fig. 3(A) ($x = 0$ system) [24–29, 37–41]. Figure 7(B) shows curve a′ and also another ZFC curve (curve c′) of an SC system. Again, the sum curve (curve a′ + c′) is very similar to the curve a + c. As the natures of SG, SC M–T ZFC curves plus the broadening, amplitude decrease of T_{M1}, T_{M2} peaks and T_{M1}, T_{M2}, T_c values all vary nonuniformly with H [4, 24–29, 37–43], T_{M1}, T_{M2} SGSC peaks can have oscillatory amplitude variation with H. In the main portion of Fig. 7(B), three arrows are shown that mark the T_c of curves c, c′, and a + c (a′ + c′). From these markings it is clearly seen that the T_c value obtained for an SGSC system from M–T curve (i.e., curve a + c (curve a′ + c′) T_c value) is much smaller than the actual T_c value (curve c (c′) T_c value). This is for the particular types of SG, SC curves shown in Fig. 7(B). Many interesting situations can arise depending on the relative T_c, T_C values ($<$, $=$, $>$) and relative SC diamagnetism, and SG magnetism magnitudes. Thus, the observed (i.e., obtained) T_C, T_{M1}, T_{M2}, T_c values of $x = 0.1$ SGSC system, given before, are approximate since, for this system, the observed M–T or M–H curve is a sum of superconducting state (supercurrent plus trapped flux contribution) and SG state (Ru frozen moments' contribution) M–T or M–H curves.

4 Concluding Remarks

In conclusion, the $Sr_2YRu_{1-x}Cu_xO_\delta$ ($\delta = 6$ or ~ 6) system is an SG for $x = 0$ and an SGSC for $0.05 \leq x \leq 0.3$. This conclusion is consistent with the results of $RuSr_2Gd_{1.5}Ce_{0.5}Cu_2O_{10-\delta}$ system [6] where SG nature and clusters have been found to coexist with superconductivity. It is also consistent with our continuing $A_2BRu_{1-x}Cu_xO_\delta$ ($A_2B = Ba_2Y$ [$T_c \sim 90$ K, $f_{sc} \sim 8\%$, $x = 0.1$], Ba_2Pr [$T_c \sim 11$ K, $f_{sc} \sim 4\%$, $x = 0.075$], Sr_2Ho [$T_c \sim 31$ K, $f_{sc} \sim 6.5\%$, $x = 0.2$]; $\delta = 6$ or ~ 6) systems' investigations and with the paired cluster model of cuprate superconductivity which assumes the presence of SG interactions and clusters in cuprate superconductors [26–29]. Actually a closer examination of $RuSr_2GdCu_2O_8$ data [5] also shows some possibility of its being an SGSC, though more work is needed to confirm this. It may be noted that in normal (non-Ru) cuprates where diamagnetism is very large and Cu^{2+} spins are presumably RVB singlet paired, it is difficult to detect the SG transition temperatures [26–29]. Further, it may be mentioned that in principle the absence of specific heat anomaly at any transition temperature can also be understood by assuming the presence of sample inhomogeneity provided that the inhomogeneity is large enough to broaden the anomaly beyond detection. This seems to be particularly important for T_c transition since even in normal (non-Ru) cuprates, like $YBa_2Cu_3O_{7-\delta}$, $\delta \sim 0$ (Y123 compound), where f_{sc} is large (~ 30–70% (due to large carrier concentration [e.g., 50% cations are Cu in Y123] and enhanced Cu–O–Cu overlap [e.g., Y123 unit cell volume (ucv) is $\sim 35\%$ smaller than the $x = 0.1$ doped SrY2116 ucv]), the T_c specific heat anomaly is either very small or absent [49, 50]. However, our EDX measurements carried out on different portions of a crystal have yielded same EDX spectrum from these portions indicating crystal's compositional homogeneity. Also, our X-ray and Raman lines are reasonably sharp. In addition, measurements carried out on several crystals have yielded reproducible results. All these facts do not favor the sample inhomogeneity explanation for our case. Similarly, the T_c transition can in principle be associated with a filamentary minority phase, instead of the $Sr_2YRu_{1-x}Cu_xO_\delta$ phase, assuming the sample to be an impure one. However, by our measurements (EDX, XRD) we have not been able to detect any magnetic or nonmagnetic impurity phase in the crystals. The $x = 0$ sample does not show any superconductivity, so it does not have any filamentary minority superconducting impurity phase (pure system). When Cu is introduced in this $x = 0$ system, no new lines develop in the XRD pattern, but the original $x = 0$ sample lines show a shift with x [Table 1], indicating a change in the lattice parameters and so incorporation of Cu in the Sr_2YRuO_6 unit cell rather than its (Cu) precipitation in the lattice as a superconducting minority impurity

phase. Raman spectrum also shows this incorporation [Table 1]. The EDX analysis supports 2116 stoichiometry for the system ($x = 0$, 0.1) [Table 2]. Also, the fact that the diamagnetic response is seen in Figs. 2, 3, 7, despite a sizable positive ($+M$) contribution from SG frozen moments, shows that any impurity phase, if responsible for T_c transition, should be present in a quantity detectable by the XRD, EDX measurements. It is actually the resistivity measurements where a filamentary contribution may exist from an undetectable amount of any impurity phase.

It may be noted that, as discussed in the following, we find that the $x = 0.1$ $T_{M1} \sim 32$ K peak (Fig. 7) seems to have no other explanation except that it is an SGSC peak. For instance, this peak cannot be attributed to PME (paramagnetic Meissner effect) presence since, though PME shows a peak near T_c, the PME peak is known to monotonically decrease in amplitude with increasing H, without any oscillatory behavior, and is observed for very low H ($\lesssim 1$ Oe) [51, 52]. Further, the $x = 0.1$ $T_{M1} \sim 32$ K peak cannot be associated to vortices that show a signature in the M–T curve, as a manifestation of the so-called J_c (critical current) peak effect, only at large H ($\sim$ kOe) when enough vortices are formed in the lattice [53, 54]. Thus, $-M$ (diamagnetic response in the $x = 0.1$ ZFC M–T curve) and SGSC peak ($x = 0.1$ $T_{M1} \sim 32$ K peak) (Figs. 2, 3, 7) both show the presence of superconductivity in $x = 0.1$ sample.

It may be further mentioned that, in principle, $-M$ can also be observed due to some other reasons like the presence of appreciably large stray $-H$ field during measurement, sudden crystal symmetry change or distortion giving rise to large anisotropy field or spin flop transition, or simultaneous presence of several impurity phases. However, we have found no evidence of any appreciable stray $-H$ field or impurity phase or crystal and magnetic structure distortions present in our sample ($x = 0.1$) or magnetometer. Also, the $x = 0$ system, prepared and investigated in the same manner as $x = 0.1$ system, does not show any diamagnetism ($-M$) plus on Cu doping ($x \neq 0$) retains its crystal and magnetic structures. SG magnetic clusters exist in both, $x = 0$ and $x = 0.1$, systems, both systems have comparable SG transition temperatures, and they both have the same monoclinic structure with comparable lattice parameters. Moreover, as we see in Fig. 7 and Table 1, $-M$ is observed for H as small as 5 Oe and x as small as 0.05 (when Cu ions are only $\sim 1.25\%$ of the total lattice cations). At these small values, any crystal or magnetic structure distortion is unlikely.

We now examine in somewhat detail the possibility of any stray field being the cause of $-M$ being observed in our measurements. The Hall probe measurements, carried out by us, show any stray (residual) field to be < 2 Oe in our SQUID magnetometer after the previous user has used it at its maximum field. This residual field also becomes zero after the system is degaussed by us, as described in Sect. 2,

before starting the measurement. Thus, we do not find any residual (trapped) magnetic field in our spectrometer. Moreover, as described in Sect. 3, $-M$ is not seen in $x = 0$ sample's M–T curve for any H. It is seen only in Cu-doped samples, like $x = 0.1$ sample. This also rules out any trapped magnetic field being the reason of $-M$ being observed, otherwise $x = 0$ sample would have also shown $-M$. In order to further ascertain that the $-M$ observed by us in $x = 0.1$ sample (Figs. 2, 3, 7) is not due to the presence of any negative remanent magnetic field in our magnetometer, we have carried out M–T measurement for $x = 0.1$ sample in $H = -10$ Oe, and the results are given in Fig. 8; there the curve a is the ZFC curve, and curve b is the FC curve. From the observed results (Fig. 8) we can rule out any negative remanent field being responsible for the observed $-M$ in our $x = 0.1$ sample as follows. If a small negative remanent field ($-H_r$) is present in the magnetometer, then when the system (sample) is zero-field cooled, it actually gets cooled in $-H_r$, and the spins get oriented along the direction of $-H_r$. Now when a positive field, say $H = +10$ Oe, is applied to the system for M measurement, a negative magnetization ($-M$) is observed if there is an anisotropy field present in the system holding the spins along $-H_r$ direction and not allowing them to rotate to $+H$ direction (spin (domain wall/domain) pinning). Thus, the observed ZFC M is negative. However when the system is field-cooled in $+H$, say $H = +10$ Oe, then since $+H$ is larger in magnitude than $-H_r$, system gets cooled in a net positive field $+(H - H_r)$, and so a positive M is observed. Thus, the observed FC M is positive. This picture thus, in principle, can explain the presence of negative ZFC M and positive FC M in a system without assuming the presence of superconductivity. However, this explanation fails for our case since in this picture if the ZFC-FC M–T measurements are done in $-H$ field, say $H = -10$ Oe, then both the ZFC M and FC M will have negative sign. This is because now both the ZFC and FC measurements will actually be done in a negative field, namely $-(H + H_r)$. Thus, for both the ZFC and FC measurements, measuring field will always be negative and will be in the direction of the anisotropy field. This will make both the ZFC M and FC M negative. However, this is not what we see in Fig. 8, where ZFC M is positive, and FC M is negative. This shows that the $-M$ observed by us in our system, e.g., in Fig. 3(B), is not due to the presence of any negative remanent field or anisotropy field in our magnetometer or sample. We now show that the results of Fig. 8 can be understood by assuming superconductivity presence in our system ($x = 0.1$). Just as in a positive field ($H = +10$ Oe), we saw positive FC M and negative ZFC M (e.g., Fig. 3(B)) and explained that on the basis of the coexisting SG and SC behaviors in the system, we can explain the results of Fig. 8 on the same basis since H is now negative ($H = -10$ Oe). More explicitly, as given before in

the discussion of Fig. 7(B), the observed M in our system ($x = 0.1$) is a sum of SG M and SC M. In a positive field, $H = +10$ Oe, in ZFC case, SC M is negative, as M produced by the supercurrent is opposite to the externally applied field and is larger in magnitude than the SG M which is positive. Thus, the net observed ZFC M is negative. In the FC case, SC M is negative but much smaller in magnitude, due to flux trapped during cooling in field, than the SG M which is positive (Fig. 7(B), inset). Thus, net observed FC M is positive. This is what has been observed in Fig. 3(B). Reverse is expected when externally applied field is negative, say $H = -10$ Oe. Thus, in $H = -10$ Oe, the observed ZFC M is expected to be positive, and the observed FC M negative. This is what is seen in Fig. 8. This thus confirms the presence of superconductivity in our sample ($x = 0.1$).

We thus see that the explanations, for seeing $-M$, based on the presence of several magnetic impurities or domain wall pinning or large anisotropy field in the lattice or a small stray negative field in the magnetometer, are not appropriate for our system ($x = 0.1$). Moreover, these explanations cannot account for a peak near the diamagnetic ($-M$) transition temperature whose amplitude oscillates and position shifts to lower T with increasing H (Fig. 7, $x = 0.1$). In addition, as has been mentioned before, not only in undoped and Cu-doped SrY2116, but in other similar systems, like undoped and Cu-doped BaY2116, BaPr2116, and SrHo2116, also we have seen SG ($x = 0$) and SGSC ($x \neq 0$) properties. In these cases also, on Cu doping ($x > 0$) the crystal (monoclinic) and magnetic (cluster SG) structures remain unchanged, but a diamagnetic response ($-M$) is observed. The only difference is that whereas in $Sr_2YRu_{1-x}Cu_xO_\delta$ the lattice parameters decrease with increasing x, reverse is the case in $Ba_2YRu_{1-x}Cu_xO_\delta$, $Ba_2PrRu_{1-x}Cu_xO_\delta$, and $Sr_2HoRu_{1-x}Cu_xO_\delta$. This indicates that whether the lattice contracts or expands, superconductivity appears on Cu doping. Thus, we see that the presence of $-M$ and SGSC peak (Figs. 2, 3, 7) both seem to indicate the $x = 0.1$ $Sr_2YRu_{1-x}Cu_xO_\delta$ system to have a superconducting nature. The results of Fig. 8 also confirm this. Therefore, in summary, we find that the $Sr_2YRu_{1-x}Cu_xO_\delta$ system is an SG for $x = 0$ and an SGSC for $x = 0.1$. The present work is competent as it is based on single-crystal data and thus is more reliable than any powder sample work. It provides a significant advancement to the fields of magnetic superconductors and ruthenocuprates. It shows that in systems showing coexistence of magnetism and superconductivity, the peak normally observed near T_c is an SGSC (or magnetic SC in general context) peak and that T_c reported for these systems is not the correct T_c and could be quite approximate. It also shows that the basic (undoped) system, SrY2116, is an SG and not an antiferromagnet as was thought earlier. Same is true for other undoped Ru (magnetic ion) containing double perovskites. The Cu-doped system is an SGSC, and other

ruthenocuprates are likely to have similar behavior. These findings are new and are expected to induce more activities in the field. They add to our understanding of ruthenocuprate and magnetic superconductor behaviors.

References

1. Maeno, Y., Hashimoto, H., Yoshida, K., Nishizaki, S., Fujita, T., Bednorz, J.G., Lichtenberg, F.: Nature **372**, 532 (1994)
2. Ling, D.C., Sheen, S.R., Tai, C.Y., Tseng, J.L., Wu, M.K., Chen, T.Y., Chien, F.Z.: In: Batlogg, B., Chu, C.W., Chu, W.K., Gubser, D.U., Müller, K.A. (eds.): Proc. 10th Anniversary HTS Workshop on Physics, Materials and Applications, p. 129. World Scientific, Singapore (1996)
3. Wu, M.K., Chen, D.Y., Chien, F.Z., Sheen, S.R., Ling, D.C., Tai, C.Y., Tseng, G.Y., Chen, D.H., Zhang, F.C.: Z. Phys. B **102**, 37 (1997)
4. Chen, D.Y., Chien, F.Z., Ling, D.C., Tseng, J.L., Sheen, S.R., Wang, M.J., Wu, M.K.: Physica C **282–287**, 73 (1997)
5. Bernhard, C., Tallon, J.L., Niedermayer, Ch., Blasius, Th., Golnik, A., Brücher, E., Kremer, R.K., Noakes, D.R., Stronach, C.E., Ansaldo, E.J.: Phys. Rev. B **59**, 14099 (1999)
6. Cardoso, C.A., Araujo-Moreira, F.M., Awana, V.P.S., Takayama-Muromachi, E., de Lima, O.F., Yamauchi, H., Karppinen, M.: Phys. Rev. B **67**, 020407(R) (2003)
7. Lynn, J.W., Keimer, B., Ulrich, C., Bernhard, C., Tallon, J.L.: Phys. Rev. B **61**, R14964 (2000)
8. Liu, R.S., Jang, L.-Y., Hung, H.-H., Tallon, J.L.: Phys. Rev. B **63**, 212507 (2001)
9. Kumagai, K., Takada, S., Furukawa, Y.: Phys. Rev. B **63**, 180509(R) (2001)
10. McLaughlin, A.C., Attfield, J.P.: Phys. Rev. B **60**, 14605 (1999)
11. Awana, V.P.S., Ansari, M.A., Gupta, A., Saxena, R.B., Kishan, H., Buddhikot, D., Malik, S.K.: Phys. Rev. B **70**, 104520 (2004)
12. Felner, I., Nowik, I., Tsindlickt, M.I., Yuli, O., Asulin, I., Millo, O., Awana, V.P.S., Kishan, H., Balamurugan, S., Takayama-Muromachi, E.: Phys. Rev. B **76**, 144514 (2007)
13. Blackstead, H.A., Yelon, W.B., Kornecki, M., Smylie, M.P., Cai, Q., Lamsal, J., Awana, V.P.S., Balamurugan, S.: Phys. Rev. B **76**, 094507 (2007)
14. Lynn, J.W., Chen, Y., Huang, Q., Goh, S.K., Williams, G.V.M.: Phys. Rev. B 014519 (2007)
15. Donohue, P.C., McCann, E.L.: Mater. Res. Bull. **12**, 519 (1977)
16. Greatrex, R., Greenwood, N.N., Lal, M., Fernandez, I.: J. Solid State Chem. **30**, 137 (1979)
17. Battle, P.D., Jones, C.W.: J. Solid State Chem. **78**, 108 (1989)
18. Battle, P.D., Macklin, W.J.: J. Solid State Chem. **54**, 245 (1984)
19. Battle, P.D., Goodenough, J.B., Price, R.: J. Solid State Chem. **46**, 234 (1983)
20. Battle, P.D., Macklin, W.J.: J. Solid State Chem. **52**, 138 (1984)
21. Doi, Y., Hinatsu, Y.: J. Phys. Condens. Matter **11**, 4813 (1999)
22. Anderson, M.T., Greenwood, K.B., Taylor, G.A., Poeppelmeier, K.R.: Prog. Solid State Chem. **22**, 197 (1993)
23. Izumiyama, Y., Doi, Y., Wakeshima, M., Hinatsu, Y., Shimojo, Y., Morli, Y.: J. Phys. Condens. Matter **13**, 1303 (2001)
24. Srivastava, J.K., Ferreirinho, J., Ramakrishnan, S., Campbell, S.J., Chandra, G., Vijayaraghavan, R.: Hyperfine Int. **68**, 279 (1991) (Erratum: Hyperfine Int. **77**, 201 (1993))

25. Srivastava, J.K., Treutmann, W., Untersteller, E.: Phys. Rev. B **71**, 174429 (2005)
26. Srivastava, J.K.: Phys. Status Solidi (b) **210**, 159 (1998)
27. Srivastava, J.K.: In: Narlikar, A. (ed.): Studies of High Temperature Superconductors: Advances in Research and Applications, Vol. 29, p. 113. Nova Science, New York (1999)
28. Srivastava, J.K.: In: Srivastava, J.K., Rao, S.M. (eds.): Models and Methods of High-T_c Superconductivity: Some Frontal Aspects, Vol. 1, p. 9. Nova Science, New York (2003)
29. Srivastava, J.K.: cond-mat/0508292 (Aug. 2005) [http://arxiv.org/abs/cond-mat/0508292]
30. Srivastava, J.K., Morimoto, S., Ito, A.: Hyperfine Int. **54**, 717 (1990)
31. Srivastava, J.K., Hammann, J., Asai, K., Katsumata, K.: Phys. Lett. A **149**, 485 (1990)
32. Wenger, L.E., Keesom, P.H.: Phys. Rev. B **11**, 3497 (1975)
33. Wenger, L.E., Keesom, P.H.: Phys. Rev. B **13**, 4053 (1976)
34. Ho, J.C., Dandekar, D.P.: J. Mater. Sci. Lett. **8**, 169 (1989)
35. Falge, R.L. Jr., Wolcott, N.M.: J. Low Temp. Phys. **5**, 617 (1971)
36. Señarís-Rodríguez, M.A., Goodenough, J.B.: J. Solid State Chem. **118**, 323 (1995)
37. Verbeek, B.H., Mydosh, J.A.: J. Phys. F **8**, L109 (1978)
38. Kleiman, R.N., Maartense, I., Williams, G.: Phys. Rev. B **26**, 5241 (1982)
39. Srivastava, J.K., Jéhanno, G., Muraleedharan, K., Kulkarni, J.A., Marathe, V.R., Darshane, V.S., Vijayaraghavan, R.: Hyperfine Int. **28**, 519 (1986)
40. Srivastava, J.K., Muraleedharan, K., Vijayaraghavan, R.: Phys. Status Solidi (b) **140**, K47 (1987)
41. Srivastava, J.K., Kulkarni, J.A., Ramakrishnan, S., Singh, S., Marathe, V.R., Chandra, G., Darshane, V.S., Vijayaraghavan, R.: J. Phys. C **20**, 2139 (1987)
42. Iye, Y.: In: Narlikar, A. (ed.): Studies of High Temperature Superconductors: Advances in Research and Applications, Vol. 2, p. 210. Nova Science, New York (1989)
43. Marbach, G., de Vries, J.W.C., Klee, M., Passing, H., Stotz, S.: In: Narlikar, A. (ed.): Studies of High Temperature Superconductors: Advances in Research and Applications, Vol. 5, p. 171. Nova Science, New York (1990)
44. Tallon, J.L., Loram, J.W., Williams, G.V.M., Bernhard, C.: Phys. Rev. B **61**, R6471 (2000)
45. Nakamura, K., Park, K.T., Freeman, A.J., Jorgensen, J.D.: Phys. Rev. B **63**, 024507 (2000)
46. Felner, I., Kowitt, M., Lehavi, Y., Ben-Dor, L., Wolfus, Y., Barbara, B., Nowik, I.: Physica C **153–155**, 898 (1988)
47. Norling, P., Svedlindh, P., Nordblad, P., Lundgren, L., Przyslupsky, P.: Physica C **153–155**, 314 (1988)
48. Giovannella, C., Fruchter, L., Chappert, C.: Physica C **153–155**, 326 (1988)
49. Gmelin, E.: In: Narlikar, A. (ed.): Studies of High Temperature Superconductors: Advances in Research and Applications, Vol. 2, p. 95 Nova Science, New York (1989)
50. Junod, A.: In: Ginsberg, D.M. (ed.): Physical Properties of High Temperature Superconductors II, p. 13. World Scientific, Singapore (1990)
51. Papadopoulou, E.L., Nordblad, P., Svedlindh, P., Schöneberger, R., Gross, R.: Phys. Rev. Lett. **82**, 173 (1999)
52. Gardchareon, A., Mathieu, R., Jönsson, P.E., Nordblad, P.: Phys. Rev. B **67**, 052505 (2003)
53. Valenzuela, S.O., Maiorov, B., Osquiguil, E., Bekeris, V.: Phys. Rev. B **65**, 060504(R) (2002)
54. Kwok, W.K., Fendrich, J.A., van der Beek, C.J., Crabtree, G.W.: Phys. Rev. Lett. **73**, 2614 (1994): Actually a dip is seen in χ (or M) vs. T curve, but the edge of the dip appears like a peak